Quarterly Journal of the Royal Meteorological Society *Q. J. R. Meteorol. Soc.* 140: 729–737, April 2014 DOI:10.1002/qj.2191

RMetS
Royal Meteorological Society

Long-lived Rossby wave trains as precursors to strong winter cyclones over Europe

V. Wirth* and J. Eichhorn

Institute for Atmospheric Physics, Johannes Gutenberg-Universität, Mainz, Germany

*Correspondence to: V. Wirth, Institute for Atmospheric Physics, Johannes Gutenberg-Universität, Becherweg 21, 55126 Mainz, Germany. E-mail: vwirth@uni-mainz.de

The statistical connection between strong surface cyclones over Europe and long-lived upper-tropospheric Rossby wave trains is examined for the Northern Hemisphere winter season using 45 years of reanalysis data. Dates are selected for which the surface pressure anomaly over Central Europe is below a threshold yielding the 5% of lowest values. Composites of upper tropospheric meridional wind for these dates (including a lead or lag in time) display clear signs of a wave train. The composite wave train lives for over two weeks and propagates eastward over more than 360° longitude. The phase speed of individual lows and highs, by contrast, is close to zero and the same is true for the composite surface low. There is a pronounced northward shift of the wave train as it propagates over the North American East coast. Although this composite wave train is statistically highly significant, there is large scatter about the mean. An index is defined that quantifies the similarity of the upper-tropospheric meridional wind pattern for an arbitrary date with the composite wave train for a certain lead or lag. Given large positive values of the index, there is an enhanced probability of a strong surface cyclone over Central Europe a few days later. Comparison with a previous study focusing on Pacific cyclones shows noteworthy differences.

Key Words: Rossby waves; wave packets; strong winter cyclones; statistical predictability; composite analysis

Received 23 January 2013; Revised 28 April 2013; Accepted 16 May 2013; Published online in Wiley Online Library 26 July 2013

1. Introduction

Low-pressure systems and associated severe weather over Europe are sometimes associated with long-lived Rossby wave trains in the upper troposphere. One such case occurred in the summer of 2002, when on August 10–13 a surface cyclone crossed Europe on a so-called Vb track (van Bebber, 1891), leading to heavy precipitation over parts of Central Europe and catastrophic flooding of the river Elbe (Grazzini and van der Grijn, 2002; Ulbrich *et al.*, 2003a,b). During the days preceding the event, the upper tropospheric flow featured clear signs of a Rossby wave train (Sharpio and Thorpe, 2004). As shown in Figure 1, the wave train started some 12 days earlier (around August 1) off the coast of Japan and circumnavigated the major part of the globe until it reached Central Europe around August 10. The sequence of positive and negative wind maxima on this Hovmöller diagram features the well-known patterns of a zonally propagating Rossby wave train including 'downstream development', i.e. with the group velocity being much larger than the phase velocity (Hovmöller, 1949; Chang, 1993; Chang and Yu, 1999; Glatt *et al.*, 2011).

The connection between a planetary-scale coherent Rossby wave train and a synoptic-scale severe weather event is of significant interest. It suggests potential predictability of the weather event on the time-scale of the Rossby wave train, which is sometimes one week or even longer. Apparently, current numerical weather prediction models sometimes have difficulties in extending skilled forecasts of significant weather into this medium-range time frame. For instance, the forecast of the heavy precipitation event of August 2002 by the different meteorological services proved to be a limited success even at rather short lead times (3–4 days: Gibson, 2003). One is tempted to conclude that there is significant room for improvement.

This state of affairs calls for more work studying the connection between long-lived Rossby wave trains and shorter, more local severe weather events. In the present article we take a first step in this direction by studying the statistical connection between strong winter cyclones over Europe and preceding long-lived upper-level Rossby wave trains. We shall quantify the properties of these Rossby wave trains and explore to what extent they can be exploited for statistical prediction. We deliberately focus our attention on strong surface cyclones as representatives of a 'significant synoptic event', because these are less localized than high wind or heavy precipitation events and, therefore, more amenable to straightforward analysis. In many aspects our method of analysis is similar to that of Chang (2005). However, our focus is on European cyclones rather than West Pacific cyclones and this gives rise to important differences in the results.

The plan of the article is as follows. The source of data and the selection of the strong cyclone sample are discussed in Section 2. In

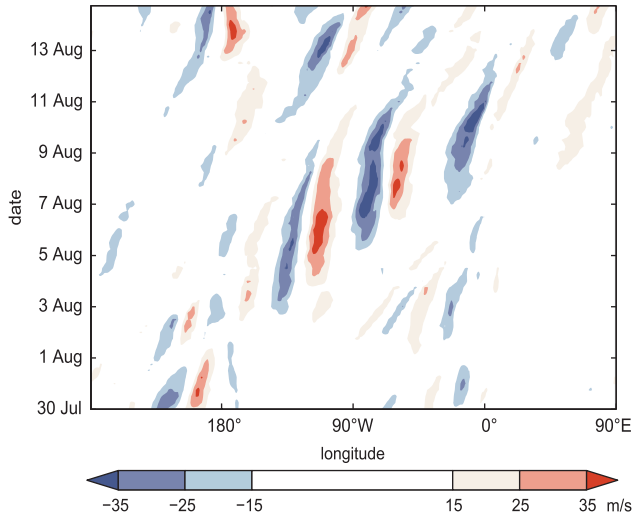

Figure 1. Hovmöller diagram of the 250 hPa meridional wind (in m s^{-1}) during the episode 30 July–15 August 2002. The diagram was obtained by averaging over the latitude band 40°N–60°N.

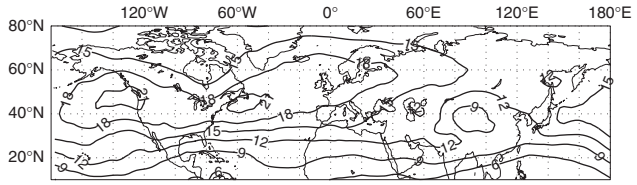

Figure 2. Diagnostics for the transient eddy activity at 300 hPa, averaged over the 45 winters of the ERA-40 dataset. The plot shows the temporal standard deviation of v' (in m s^{-1}, contours every 3 m s^{-1}).

Section 3 we present composite wave trains conditioned on strong surface cyclones over Europe and examine their properties. The sensitivity of our results with respect to the geographical location of the strong surface cyclone is investigated in Section 4. Section 5 addresses the question of to what extent these connections can be exploited for statistical prediction. Finally, we provide a discussion and our conclusions in Section 6.

2. Data and sample selection

2.1. The data

We use data from the ERA-40 project spanning the time September 1957–February 2002 (Uppala *et al.*, 2005). The data were retrieved on a longitude–latitude grid with 2.5° × 2.5° resolution. The fields used in this study are surface pressure p_s and meridional wind v on standard pressure levels for the winter season (i.e. December, January and February, henceforth abbreviated as DJF). The retrieved data have a 12 hourly resolution, yielding a total of slightly over 8000 dates. Anomalies p_s' and v' were computed following Chang and Yu (1999) by subtracting the seasonal mean for each individual winter. This effectively gets rid of the stationary component of the flow and focuses on the transient phenomena. Our time-lag analysis required a few data from November and March; anomalies for those autumn and spring dates were computed by subtracting the DJF-mean for the corresponding individual winter season.

In order to characterize the transient eddy activity in our dataset, Figure 2 shows the temporal standard deviation of v' over 45 winters. The two relative maxima correspond to the storm tracks over the Pacific and Atlantic Oceans, respectively. This result is very similar to earlier analyses, although the latter made use of considerably shorter time series (see e.g. Chang, 1993; Chang and Yu, 1999).

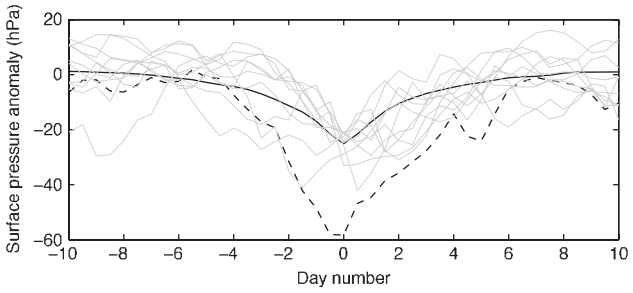

Figure 3. Time series of p_s' for the sample of 'strong surface cyclone events' at grid point $\mathbf{x}_0$ = (10°E, 50°N). The x-axis denotes the time (in days) relative to day 0; day 0 is the day upon which the selection has been made. The thin grey lines represent 10 random picks from the sample, the dashed line is the event with the lowest p_s' on day 0 and the black solid line is the sample mean.

2.2. Selection of strong surface cyclones

In order to select a data sample containing 'strong surface cyclones over Central Europe', we decided to follow the simple algorithm of Chang (2005). Essentially, we analyzed the time series of p_s' at a reference grid point $\mathbf{x}_0$ and chose those 5% of all dates containing the lowest values of p_s'. The corresponding threshold value of p_s' is called p_0'. This algorithm selects approximately 400 dates from our dataset, yielding satisfying statistics. We also tried a more sophisticated algorithm looking for true relative minima in surface pressure, but the results turned out to be very similar (albeit statistically less robust). We are, therefore, confident that our 'low-pressure anomaly sample' provides a reasonable representation of strong surface cyclones at point $\mathbf{x}_0$ and we shall refer to these cyclones as 'target cyclones' in the following. At one point we shall also consider a sample containing strong surface *anticyclones*; the latter is defined in an analogous manner, i.e. by selecting the 5% of all dates containing the *highest* values of p_s'. Unless otherwise specified, we chose $\mathbf{x}_0$ = (10°E, 50°N).

Figure 3 shows time series of p_s' for a random selection of 10 target cyclones. The same plot also provides the average over the entire strong cyclone set, as well as the time series for the deepest target cyclone. Apparently, there is strong scatter about the average. This suggests that the composites we consider in the following sections have to be interpreted with care, as individual cases may differ strongly from the composite picture.

3. Composite Rossby wave train

We shall now examine the typical patterns – in both space and time – for those events associated with a target cyclone at the reference point $\mathbf{x}_0$ on day 0. To this end we computed time-lagged composites $\hat{\psi}^{(d)}$, where ψ represents the variable to be considered and $d = -10, -9, \ldots, +10$ denotes the time lag in days. At each grid point, $\hat{\psi}^{(d)}$ was obtained by averaging ψ over all dates i for which p_s' at the grid point $\mathbf{x}_0$ on day $(i - d)$ satisfies the criterion to belong to the 'strong surface cyclones' sample.

The results for the upper-level meridional wind and surface pressure are shown in Figure 4. Apparently, there is a distinct upper-level wave train (left column), which propagates eastward as time increases. On day 0 the sequence of anomalously low and high values of $\hat{v}'^{(0)}$ extends from North America over the North Atlantic and Europe well into Central Asia, with maximum amplitudes over the Eastern Atlantic and Europe. In midlatitudes, the wave train has approximately zonal wave number 5. Regarding the evolution in time, a wave signal in the upper troposphere is visible as early as day −9 over the Eastern North Pacific. It remains rather weak until day −6, when it strengthens significantly. Subsequently, the wave train gradually strengthens in amplitude while travelling eastward across North America and the North Atlantic, reaching its strongest amplitude around day 0. Later, it propagates across Asia, where it appears to split into two

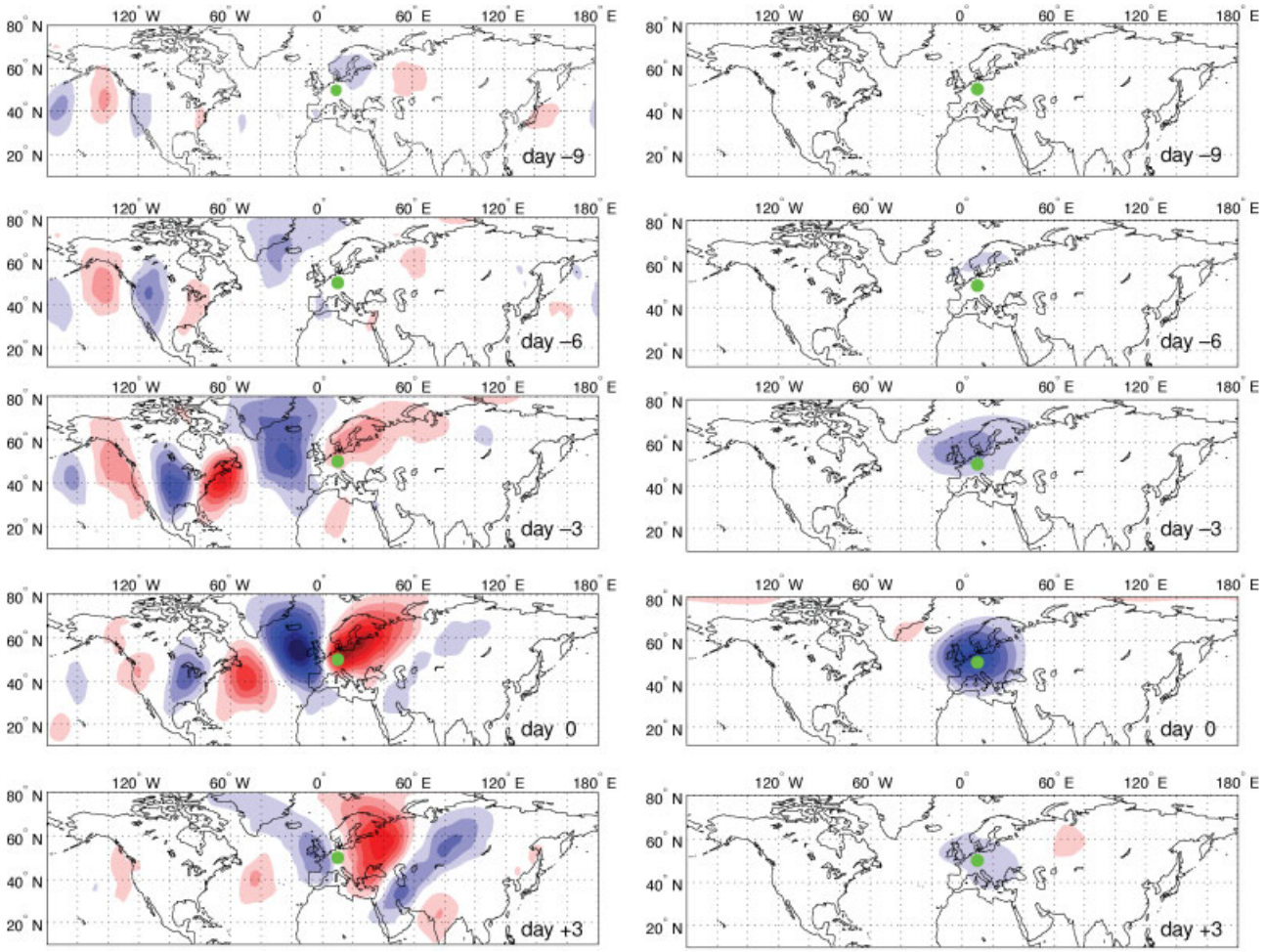

Figure 4. Lagged composites for the 300 hPa meridional wind $\hat{v}^{(d)}$ (in m s^{-1}, left column) and for the surface pressure anomaly $\hat{p}^{(d)}$ (in hPa, right column). The lag d (in days) is given in the lower right corner of each panel. The contour interval in the left column is 2 m s^{-1}, while in the right column it is 4 hPa; in both columns the zero contour is omitted and positive (negative) contours are red (blue). The green dot in each panel depicts the grid point $\mathbf{x}_0$, which is used to identify strong surface cyclones on day 0.

branches around day +2 and decays to very low amplitudes after day 6.

On day 0 there is a strong surface-pressure anomaly (Figure 4, right column) associated with the composite wave train. The low-pressure anomaly is centred about the reference point $\mathbf{x}_0$. This is not surprising but rather by design, because our composite was conditioned on low surface pressure on the reference point. The location of the surface pressure hardly changes with time lag, but its amplitude is much weaker for moderate (both positive and negative) time lags in comparison with day 0. This is consistent with the composite evolution of p_s in Figure 3 (thick line), where the average pressure perturbation drops below −10 hPa for $-2 \le d \le 2$ only.

We tested the significance of the wave-train patterns from the left column of Figure 4 using a Monte Carlo technique similar to that of Martius *et al.* (2008). In this context it is important to note that the number of independent cyclones in our cyclone sample is significantly smaller than the size of this dataset (which is approximately 400). The reason is that a single cyclone is generally associated with several (consecutive) dates in our dataset, owing to its rather low phase speed. Taking this effect into account, the number of independent cyclones in our sample turned out to be 164. We then chose the maps of v' at 300 hPa from 164 random dates and computed the corresponding composite $\hat{v}'$. We repeated this procedure 20 000 times and determined the 0.5th percentile $\hat{v}'_{0.5\%}$ and the 99.5th percentile $\hat{v}'_{99.5\%}$ of the corresponding frequency distribution at every grid point. The quantity $|\hat{V}'|_{1\%} = 0.5(\hat{v}'_{99.5\%} - \hat{v}'_{0.5\%})$ is then interpreted as the amplitude of $|\hat{v}'|$ that would be exceeded with a probability of 1% in a random composite. The field is shown in Figure 5. Apparently, $|\hat{V}'|_{1\%}$ has substantial spatial variability,

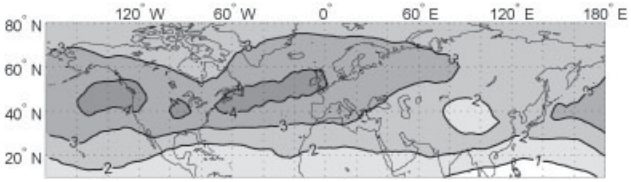

Figure 5. Amplitude $|\hat{V}'|_{1\%}$ (in m s^{-1}), corresponding to the magnitude of the meridional wind perturbation at 300 hPa that occurs in random composites with a likelihood of 1%.

with a pattern closely resembling the standard deviation of v' from Figure 2; typical values are slightly above 4 m s^{-1} in the storm track regions, with smaller values in the surrounding areas. It follows that values of $\hat{v}^{(k)} \ge 4\,\mathrm{m\,s^{-1}}$ are significant at the 1% level (an additional analysis indicates that values of $\hat{v}^{(k)} \ge 3\,\mathrm{m\,s^{-1}}$ are significant at the 5% level). We conclude that the wave train shown in the left column of Figure 4 is statistically highly significant.

Both the individual patterns of high and low values of $\hat{v}$ in Figure 4 and the wave group as a whole move eastward, but the former at a much slower pace than the latter. In other words, both phase and group velocity are eastward, but the phase velocity is much smaller than the group velocity. For this reason, a non-zero pattern remains when averaging over subsequent time lags as follows:

$$\overline{V} = \frac{1}{21} \sum_{d=-10}^{+10} \hat{v}^{(d)} \,. \qquad (1)$$

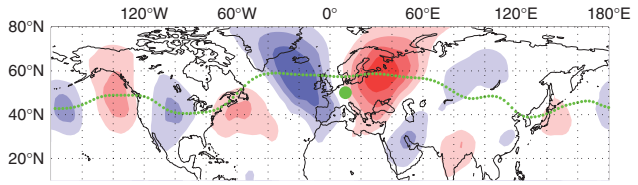

Figure 6. Time-average Rossby wave train $\overline{V}$ (in $\mathrm{m\,s^{-1}}$) at 300 hPa as defined in (1). The contour interval is $2\,\mathrm{m\,s^{-1}}$, the zero contour is omitted and positive (negative) contours are red (blue). The dotted green line depicts the centre latitude ϕ_0 defined in (2). The thick green dot denotes the reference point $\mathbf{x}_0$.

As can be seen in Figure 6, the field $\overline{V}$ captures many of the essential features of the composite wave train throughout its live time in a compact manner. Amongst other things, the figure indicates that the wave train undergoes substantial excursions in the meridional direction on its way around the Earth. To work out this feature more explicitly, we define a centre latitude ϕ_0 as follows. First the envelope $\mathcal{E}$ of the wave train was computed using the technique of Zimin *et al.* (2003), where only zonal wave numbers $s = 1, \ldots, 15$ were accounted for. Then, ϕ_0 at each longitude is obtained through

$$\phi_0 = \frac{\int \phi\, \mathcal{E}^4 \,\mathrm{d}\phi}{\int \mathcal{E}^4 \,\mathrm{d}\phi}, \tag{2}$$

where the integration extends from $\phi = 20{-}80°\mathrm{N}$. The result is depicted as the green dotted line in Figure 6. It captures the mean latitudinal position of the wave train well, except in regions with a split wave train. Figure 6 shows that the composite wave train moves meridionally from around 40°N over North America to around 60°N over the North Atlantic and Europe; far upstream over the Pacific Ocean the wave train is positioned around 50°N with an arch shape, suggesting a ridge of the basic flow over the eastern Pacific Ocean (cf. Hoskins and Hodges, 2002).

An important technique to visualize the spatio-temporal behaviour of Rossby wave trains is the so-called Hovmöller diagram (Hovmöller, 1949; Glatt *et al.*, 2011). In the conventional version of the Hovmöller diagram, the fields are averaged over a fixed band of latitudes and then plotted against time. However, since our composite Rossby wave train has a substantial component of propagation in the meridional direction, it appears desirable that the meridional average somehow accounts for these latitudinal excursions. We, therefore, computed the latitudinal average over the interval $[\phi_0 - 10°, \phi_0 + 10°]$. The corresponding Hovmöller diagram for the composite Rossby wave train from Figure 4 is shown in Figure 7(a). The patterns of minima and maxima reflect what has been pointed out before, namely that both phase and group velocity are eastward, with the phase velocity being much smaller than the group velocity. Before day −6, the wave signal is weak. Around day −6, a significant wave train appears over the eastern Pacific and western North America, propagating eastwards with rather large group velocity (approximately 45° per day). Later, between day −2 and day +3, the group velocity is somewhat smaller (approximately 30° per day) and the same is true for the phase velocity. By the time the wave train reaches Central Asia (around 100°E), the wave amplitude decays to rather small amplitudes. Comparison with the left column of Figure 4 indicates that this is, to some degree, due to the latitudinal average over the two branches of the split wave train leading to negative interference. Further downstream, as the wave train reaches the Western Pacific, the two branches merge and the wave train becomes visible again in the Hovmöller plot. It crosses the date line around day +7 and propagates well into the Eastern Pacific.

Incidentally, we repeated the same analysis for the 'strong anticyclones composite'. The resulting Hovmöller diagram is shown in Figure 7(b). Overall, the patterns are similar, with positive and negative values exchanged. However, there are interesting differences regarding the details. For instance, the upstream wave train is significantly weaker until around day −3. Also, between day +1 and +5 the phase velocity is westward for the anticyclones composite, in distinct contrast with the cyclones composite. We conclude that, while on a superficial level both cyclones and anticyclones are associated with upstream wave trains, subtle differences in the composite patterns suggest possibly important differences in the underlying dynamics.

Vertical sections of the perturbation meridional wind for the cyclonic composites are shown in Figure 8. Generally, lines of constant phase tilt westwards with height (by some 10° longitude over the depth of the troposphere) in the large-amplitude part of the wave train. The phase tilt is less pronounced in the leading and trailing parts of the wave train. Interestingly, the wave signal reaches down to the lower troposphere as early as day −6. As the wave train propagates eastward, the lower tropospheric signal is stronger over the North American continent than further east on the Western Atlantic. The lower tropospheric signal becomes large between day −2 and day +1. By design, there is a strong surface signature on day 0, because the target cyclone on day 0 is associated with strong surface winds in the meridional direction. The surface signature becomes rather weak after day +3 and vanishes all together around day +6 (not shown).

4. Geographical dependence

To what extent do our results depend on the location of the reference point $\mathbf{x}_0$? To address this question, we repeated the analysis at four additional points $\mathbf{x}_0 =$ (10°E, 60°N), (20°E, 50°N), (10°E, 40°N) and (0°E, 50°N). The corresponding time average composites $\overline{V}$ are presented in Figure 9, together with the original one that was already shown in Figure 6.

The composite pattern for $\mathbf{x}_0 =$ (60°N, 10°E) (top panel) has a quite different appearance compared with the one considered so far (middle panel) and its upstream extension is significantly less. On the other hand, all three patterns associated with a cyclone at 50°Nlook quite similar, showing a nice wave train; in particular, they all feature a strong northward shift as they leave the North American continent. Interestingly, East European cyclones (second panel from the bottom) are associated with an upstream wave train which (in the time average) is even stronger than the one studied in the previous section (middle panel). South European cyclones (bottom panel) are associated with a wave train that has a fairly strong amplitude in the southern branch of the split Asian wave train.

5. Statistical predictability

By construction, our composites are simple averages for a specific selection of dates. Generally, individual cases deviate from the average picture despite the fact that the average wave train is statistically highly significant. The scatter about the average is particularly relevant as far as statistical predictability is concerned. This section examines these questions. Note that we consider the statistical predictability of strong winter cyclones from upper-level Rossby wave precursors as a property of the flow; it is not intended actually to forecast those cyclones using such a statistical technique.

We define an index $I^{(d)}$, which quantifies the similarity of an arbitrary map of v' when compared with the composite $\hat{v}^{(d)}$ for some given value of d:

$$I^{(d)} := \frac{\langle v', \hat{v}^{(d)} \rangle}{\sqrt{\langle \hat{v}^{(d)}, \hat{v}^{(d)} \rangle}}, \tag{3}$$

where

$$\langle f, g \rangle := \frac{\sum_{i=1}^{N} f_i g_i \cos\phi_i}{\sum_{i=1}^{N} \cos\phi_i} \tag{4}$$

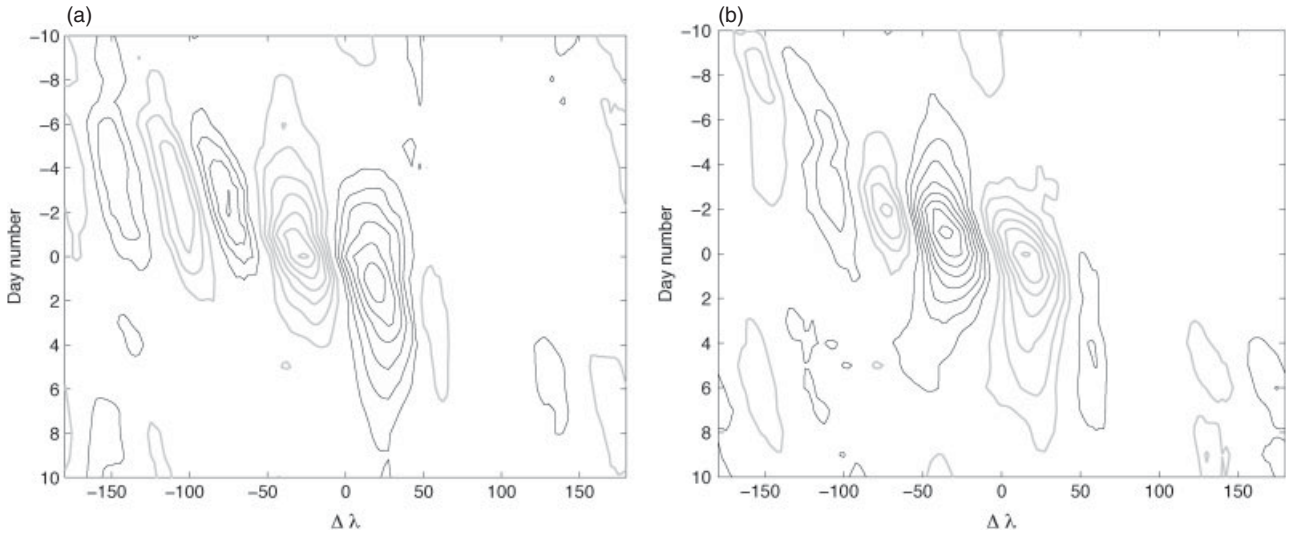

Figure 7. Hovmöller diagram for the composits $\hat{v}^{(d)}$ at 300 hPa, for (a) the strong cyclones sample and (b) the strong anticyclones sample. The contour interval is 2 m s^{-1}, positive contours are black and negative contours grey and the zero contour is omitted. The abscissa $\Delta\lambda$ denotes the distance in longitude (in degrees) from $\mathbf{x}_0$.

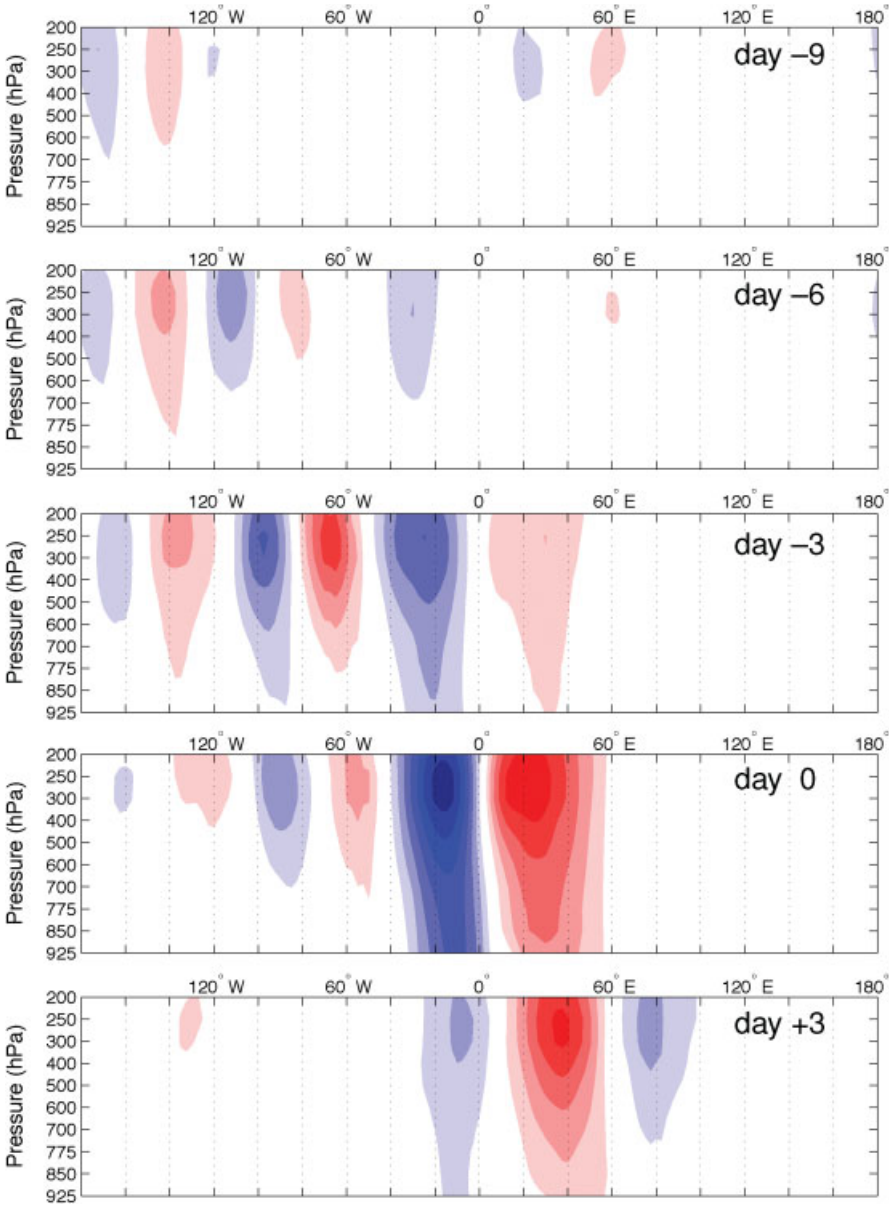

Figure 8. Vertical sections of $\hat{v}^{(d)}$ for selected lags d. The field plotted is an average in latitude over the interval $[\phi_0 - 10°, \phi_0 + 10°]$. The contour interval is 2 m s^{-1}, the zero contour is omitted and positive (negative) values are red (blue).

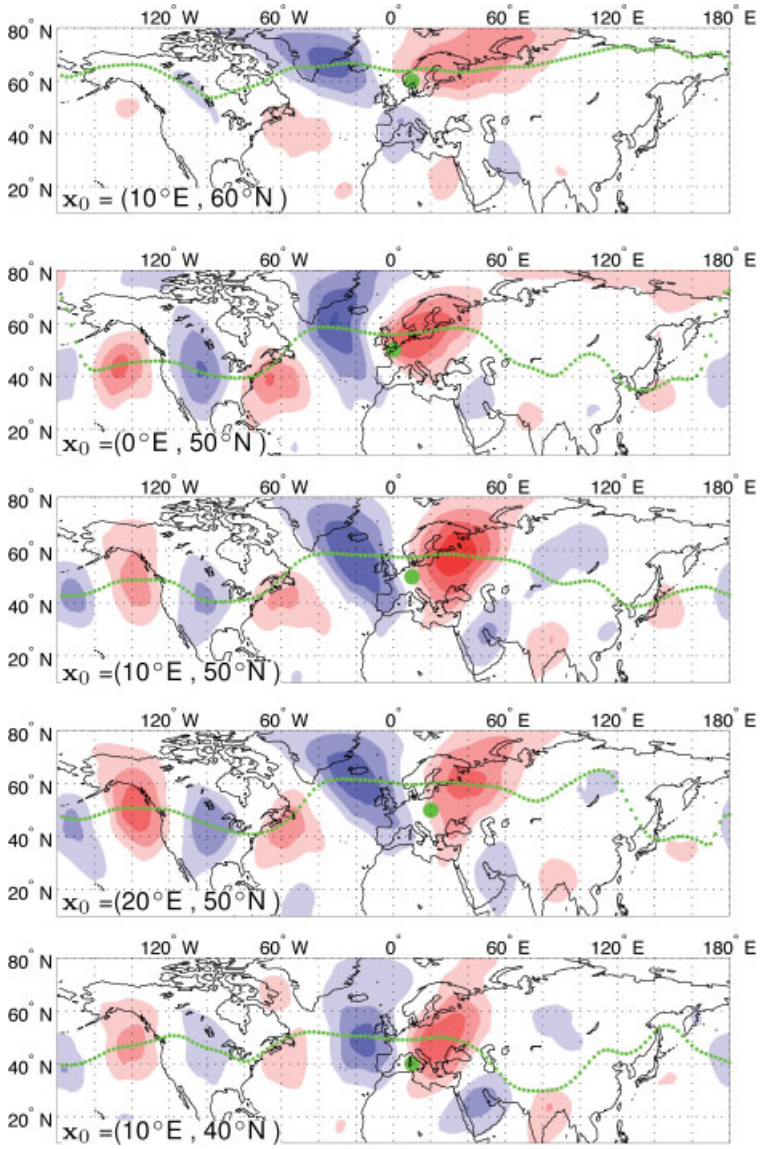

Figure 9. Time-average composites $\overline{V}$ at 300 hPa for five different reference points $\mathbf{x}_0$ (given in the lower left of each panel). Plot conventions are as in Figure 6.

represents an inner product between two fields $f(\lambda, \phi)$ and $g(\lambda, \phi)$, with the sum i running over all grid points between 20 and 80°N and with ϕ_i denoting the latitude of the respective grid point. If v' happens to be equal to $\hat{v}^{(d)}$, the index $I^{(d)}$ is equal to $\sqrt{\langle \hat{v}^{(d)}, \hat{v}^{(d)} \rangle}$, which is the spatial standard deviation.

Looping through all (i.e. approximately 8000) dates, we computed $I^{(d)}$ for each date as well as p'_s at the corresponding day 0 (i.e. $-d$ days later). The resulting scatter diagram is shown in Figure 10 for $d = -6$ (panel a) and $d = -3$ (panel b). To the extent that $v^{(d)}$ is a good predictor for p'_s on day 0, one would expect a good correlation between $I^{(d)}$ and p'_s. Apparently, the correlation is far from perfect; rather, there is strong scatter. Nevertheless, on average the two quantities are linearly correlated, with the correlation being significantly larger for $d = -3$ than for $d = -6$. We grouped the data into p'_s bins and computed the mean value for $I^{(d)}$ in each bin as well as the standard error (Press *et al.*, 1992). For intermediate and strong cyclones on day 0 (i.e. for $p'_s \leq -10$ hPa), the mean value of $I^{(d)}$ is different from zero, with the difference being highly significant for $d = -3$ and marginally significant for $d = -6$. This illustrates again that the averages (e.g. our composites in the left panel of Figure 4) are statistically significant. At the same time, the large scatter about the mean shows that the sample averages are formed from individual cases with rather different values of $I^{(d)}$.

So far we have shown that, given a strong surface cyclone at the reference point on day 0, there is a statistically significant Rossby wave train *a few days earlier*. From the point of view of statistical prediction, a different question is more relevant: Observing a strong upstream Rossby wave train on a given day, what is the chance of obtaining a strong surface cyclone at the reference point *a few days later*? By definition, the chance to observe a strong surface cyclone on a given day in the total sample of dates is 5%. So the above question can be reformulated as follows: Given that one observes a strong Rossby wave train on a certain day, by what factor is the likelihood of occurrence of a strong surface cyclone a few days later enhanced (compared with the above 5%)?

To address this question, we selected only those dates from our total sample of dates for which the value of $I^{(d)}$ lies in the top 5th percentile (20th percentile). For each of these dates we computed p'_s at the same date as well as a few days earlier and later. This allowed us, for each time lag, to compute the percentage of cases exceeding the threshold value p'_0. Normalizing with respect to 5%, one obtains the factor of increase in likelihood for a strong surface cyclone by selecting cases with large index $I^{(d)}$. The corresponding time series are shown as the upper pair of lines in Figure 11 for $d = -6$ (panel a) and $d = -3$ (panel b). As one may expect, the factor maximizes around day $|d|$ in all cases. In the top 5% sample (solid lines), the increase in relative frequency on day $|d|$ is around 2.8 for $d = -6$ and around 5.1 for $d = -3$; in the top 20% sample (dashed lines), the increase in relative frequency on day $|d|$ is around 2.0 for $d = -6$ and around 2.8 for $d = -3$.

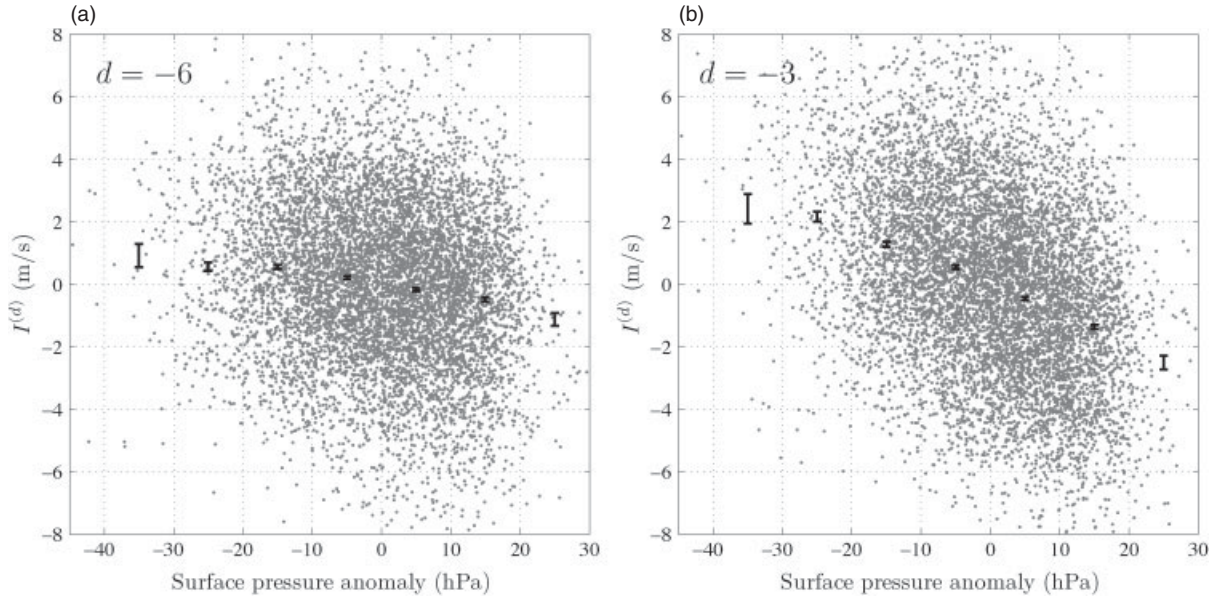

Figure 10. Scatter diagram ploting the index $I^{(d)}$ for all dates against surface pressure anomaly p'_s, $|d|$ days later: (a) $d = -6$ and (b) $d = -3$. The error bars are centred about the mean value of $I^{(d)}$ within each 10 hPa bin for p'_s; the size of the error bars indicates the standard error $\pm\Delta I^{(d)}$, where $\Delta I^{(d)}$ is equal to the standard deviation of all points within the bin divided by the square root of the number of points within the bin.

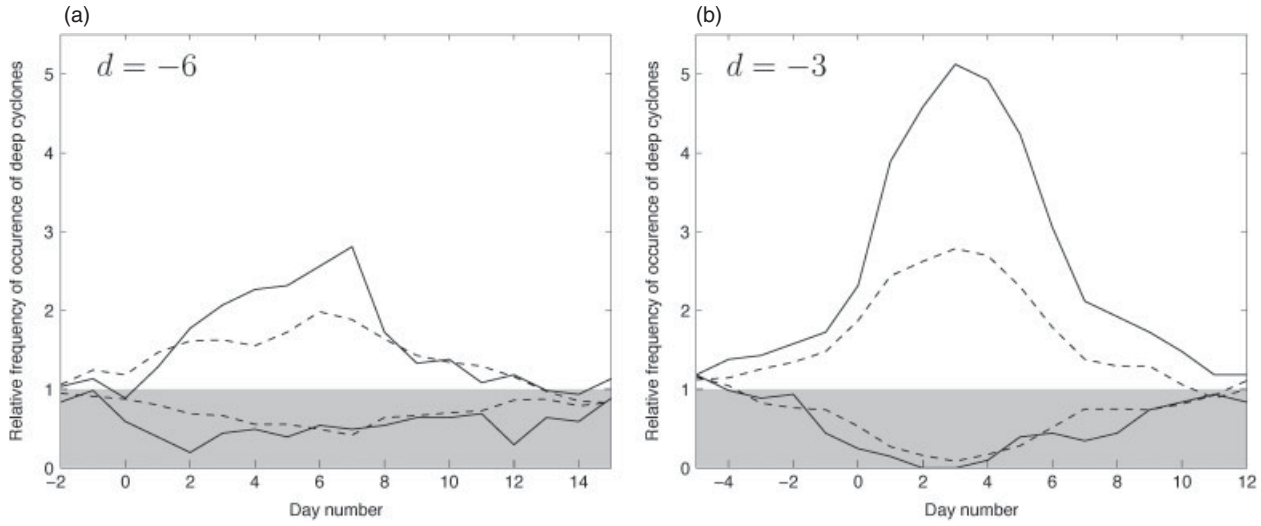

Figure 11. Time evolution of the relative frequency of occurrence of deep cyclones at reference point $\mathbf{x}_0$, provided that the index $I^{(d)}$ for day 0 is in the top 5% (solid line) and top 20% (dashed line), respectively: (a) $d = -6$, (b) $d = -3$. The upper pair of lines refers to the cyclonic composites, the lower pair of lines (within the shaded region) refers to the anticyclonic composites.

We repeated the same analysis for the strong anticyclone composites, i.e. with the index $I^{(d)}$ based on the strong anticyclone sample. The result is given as the lower pair of lines in Figure 11. As one may expect, in this case the chance of occurrence of a strong cyclone is now suppressed, i.e. the resulting factor is less than one (grey shaded area). For instance, when the index $I^{(-3)}$ is in its highest 5th percentile, the chance to observe a strong surface cyclone 2 or 3 days later is virtually zero (lower solid line in panel b).

6. Discussion and conclusions

The original question motivating this work was the following: are strong surface cyclones over Europe associated with upper-level Rossby wave trains in a statistical sense and, if so, to what extent can the latter be used to predict the former? To answer this question, we performed a composite analysis involving 300 hPa meridional wind and surface-pressure data covering some 45 years.

We found that low surface pressure anomalies on a given day over a reference point in Central Europe are, indeed, preceded on average by a distinct upper-level Rossby wave train. This composite wave train (Figure 4, left column) can be detected on the upstream side as early as 9 days prior to the low surface pressure anomaly and subsequently it extends downstream for more than a week. The wave train originates close to the date line, travels eastward, reaches its strongest amplitudes over Europe and becomes weaker as it propagates across Asia. Overall, it is in existence for over two weeks while travelling eastward over more than 360° in longitude. This eastward propagation is in the sense of group velocity; the phase velocity is eastward, too, but it is much smaller than the group velocity. The smallness of the phase velocity allows one to diagnose the broad spatial features of the wave train throughout its life cycle by averaging over consecutive time lags (Figure 6).

In contrast to the upper-level wave train, the associated composite surface pressure anomaly (Figure 4, right column) is confined to the European region and much shorter lived, reaching significant amplitudes for a few days only (see also Figure 3). This suggests that the upper-level wave trains are initially independent of lower tropospheric dynamics and that the strong cyclones over Europe are somehow triggered by the wave trains.

Although the composite wave train is statistically highly significant (cf. the analysis from Figure 5), there is large scatter about the composite average for both the upper-level wave train (Figure 10) and the surface pressure (Figure 3). This tells us that, while the composites certainly indicate some average behaviour, individual cases may differ strongly and the composite picture is only a small residuum from rather different cases.

We checked the sensitivity of our results with respect to the geographical location of the target cyclones. It turns out that our results apply to cyclones located in Middle and Southern Europe, but not in Northern Europe. In addition, the exact longitudinal position of the cyclone over Europe plays a minor role.

Some features of our composites are very similar to those found in related earlier work. For instance, our composite wave train shows a clear split as it travels across Asia, featuring a northern and a southern branch (e.g. Figure 6). Although the amplitudes are weak at large positive time lags, the two branches seem to merge later on over the Western Pacific. Both these features are consistent with the results of Chang and Yu (1999) and Chang (2005). Vertical sections through our composite wave trains (Figure 8) indicate a westward tilt with height during the mature stage of the life cycle. Again, this is similar to the behaviour found by Chang (2005) and suggests that baroclinic processes do play a role.

On the other hand, certain aspects of our composites are in distinct contrast to related earlier work. Our wave trains are significantly more expanded in longitude than those in Chang (2005) and they seem to originate at an earlier time. In addition, our composite surface pressure pattern is practically stationary throughout its existence (about one week), while those of Chang (2005) move eastward with a speed of more than 10° longitude per day. Similarly, the phase speed of individual upper tropospheric troughs and ridges for our composites (Figure 7(a)) is around 2° longitude per day during the early stage of the life cycle (day −6 to day −2), slowing down to approximately 1° longitude per day during the mature stage of the life cycle (day −2 to day +3). These values are much smaller than those in Chang (2005), who found phase speeds as large as 15° longitude per day. They are also much smaller than typical phase speeds obtained in studies that examine general characteristics of upper tropospheric wave packets without any reference to surface features (e.g. Chang, 1993; Chang and Orlanski, 1993), yielding phase speeds around 10° longitude per day.

Our composite wave train undergoes a northward shift by almost 20° as it leaves North America and travels across the western North Atlantic (see Figure 6). Such a shift does not exist in the 'schematic wave guide' of Chang and Yu (1999), who addressed general characteristics of Northern Hemisphere upper tropospheric wave packets. Possibly our northward shift is a specific feature of those wave packets that happen to be associated with strong European surface cyclones a few days later. Again, care needs to be exercised when interpreting these composite wave trains. It may well be that what appears to be one continuous (in time) composite wave train is an average over distinct wave trains succeeding one another.

We also found that the occurrence of a Rossby wave train similar to the composite wave train can be taken as a predictor for strong surface cyclones over Europe in the sense that the likelihood of occurrence of such a cyclone is increased by a substantial amount (Figure 11). This is similar to the behaviour found by Chang (2005) for East Pacific cyclones, except that in our case a substantial increase in likelihood of occurrence can be predicted as early as 6 days in advance (see Figure 11(a)), while in Chang (2005) an increase of similar magnitude was obtained only some 3 days in advance.

The differences between our results and those of Chang (2005) are not surprising owing to the different location of the target cyclones. In the case of Chang (2005), the target cyclones lie close to the entrance of the Pacific storm track, i.e. just downstream of a region with strong baroclinicity and a strong upper tropospheric jet stream. On the other hand, European cyclones (our work) lie towards the end of a storm track in a region with a much weaker upper tropospheric jet stream and much further downstream relative to a baroclinic zone. Differences in the speed of the jet stream imply differences in the flow at the steering level, which renders plausible the differences in phase speed that we obtained. Apparently, the location of the target cyclone with respect to its associated storm track also seems to have an impact on statistical predictability, with European cyclones being more predictable than West Pacific cyclones.

There are a few caveats. As pointed out before, our results need to be interpreted with care, because there is large case-to-case variability and the composite average may leave important details undetected. In addition, it is not clear to what extent our results carry over to more specific composites selecting on strong wind (e.g. Hanley and Caballero, 2012) or heavy precipitation over Central Europe. Our preliminary analysis indicates that neither of these selection criteria produces Rossby wave trains as pronounced and long-lived as our present selection criterion (i.e. low surface pressure anomaly). However, this does not preclude the existence of long-lived Rossby wave trains in cases of strong wind or heavy precipitation events; in other words, a refined and more detailed analysis may uncover statistical precursor wave trains for such events also. Another point is that the present analysis does not provide much insight into the dynamical and physical mechanisms of cyclone formation through interaction with upper-level Rossby wave trains; it is even conceivable that our sample contains (and our results average over) several distinct mechanisms. In this context, it should be useful to analyze potential vorticity and diabatic heating, as in case studies such as that of Wernli *et al.* (2002). A corresponding composite statistical analysis is beyond the scope of the present article.

Despite these caveats, a number of interesting features have emerged from our study, with noteworthy differences in comparison with a similar study over a different part of the Northern Hemisphere. We consider this as a good starting point for more detailed analyses in the future.

Acknowledgements

We are grateful for stimulating discussions with Ilona Glatt, who also provided Figure 1. In addition, we sincerely thank two anonymous reviewers for their insightful comments. Part of this work was funded by the German Research Foundation in the framework of the research unit PANDOWAE. The European Centre for Medium Range Weather Forecasts (ECMWF) in Reading (UK) kindly provided the data.

References

Chang EKM. 1993. Downstream development of baroclinic waves as inferred from regression analysis. *J. Atmos. Sci.* **50**: 2038–2053.

Chang EKM. 2005. The impact of wave packets propagating across Asia on Pacific cyclone development. *Mon. Weather Rev.* **133**: 1998–2015.

Chang EKM, Orlanski I. 1993. On the dynamics of a storm track. *J. Atmos. Sci.* **50**: 999–1015.

Chang EKM, Yu DB. 1999. Characteristics of wave packets in the upper troposphere. Part I: Northern Hemisphere winter. *J. Atmos. Sci.* **56**: 1708–1728.

Gibson A. 2003. '*Precipitation forecasts for the Central-European floods, August 2002*', Technical report. Met. Office: Exeter, UK.

Glatt I, Dörnbrack A, Jones S, Keller J, Martius O, Müller A, Peters DHW, Wirth V. 2011. Utility of Hovmöller diagrams to diagnose Rossby wave trains. *Tellus* **63A**: 991–1006.

Grazzini F, van der Grijn G. 2002. Central European floods during summer 2002. *ECMWF Newsletter* **96**: 18–28.

Hanley J, Caballero R. 2012. The role of large-scale atmospheric flow and Rossby wave breaking in the evolution of extreme windstorms over Europe. *Geophys. Res. Lett.* **39**: L21 708. DOI:10.1029/2012GL053 408.

Hoskins BJ, Hodges KI. 2002. New perspectives on the Northern Hemisphere winter storm tracks. *J. Atmos. Sci.* **59**: 1041–1061.

Hovmöller E. 1949. The Trough-and-Ridge diagram. *Tellus* **1**: 62–66.

Martius O, Schwierz C, Davies HC. 2008. Far-upstream precursors of heavy precipitation events on the Alpine south-side. *Q. J. R. Meteorol. Soc.* **134**: 417–428.

Press WH, Flannery BP, Teukolsky SA, Vetterling WT. 1992. *Numerical Recipes. The Art of Scientific Computing*, 2nd edn. Cambridge University Press: Cambridge, UK; 818pp.

Sharpio MA, Thorpe AJ. 2004. THORPEX International Science Plan, WMO TD 1246.

Ulbrich U, Brücher T, Fink AH, Leckebusch GC, Krüger A, Pinto JG. 2003a. The Central European floods in August 2002. Part I: Rainfall periods and flood development. *Weather* **58**: 371–377.

Ulbrich U, Brücher T, Fink AH, Leckebusch GC, Krüger A, Pinto JG. 2003b. The Central European floods in August 2002. Part II: Synoptic causes and considerations with respect to climatic change. *Weather* **58**: 434–442.

Uppala SM, Kållberg W, Simmons AJ, Andrae U, Da Costa Bechtold V, Fiorino M, Gibson JK, Haseler J, Hernandez A, Kelly GA, Li X, Onogi K, Saarinen S, Sokka N, Allan RP, Andersson E, Arpe K, Balmaseda MA, Beljaars ACM, Van De Berg L, Bidlot J, Bormann N, Caires S, Chevallier F, Dethof A, Dragosavac M, Fisher M, Fuentes M, Hagemann S, Hólm E, Hoskins BJ, Isaksen L, Janssen PAEM, Jenne R, Mcnally AP, Mahfouf JF, Morcrette JJ, Rayner NA, Saunders RW, Simon P, Sterl A, Trenberth KE, Untch A, Vasiljevic D, Viterbo P, Woollen J. 2005. The ERA-40 re-analysis. *Q. J. R. Meteorol. Soc.* **131**: 2961–3012.

van Bebber WJ. 1891. Die Zugstrassen der barometrischen Minima. *Meteorol. Zeitschrift* **8**: 361–366.

Wernli H, Dirren S, Liniger M, Zillig M. 2002. Dynamical aspects of the life cycle of the winter storm 'Lothar' (24–26 December 1999). *Q. J. R. Meteorol. Soc.* **128**: 405–429.

Zimin AV, Szunyogh I, Patil DJ, Hunt BR, Ott E. 2003. Extracting envelopes of Rossby wave packets. *Mon. Weather Rev.* **131**: 1011–1017.

